Protein paper from exfoliated Eri silk nanofibers

Yujia Liang^{1#} Benjamin J. Allardyce^{1#}, Sanjeeb Kalita¹, Mohammad G. Uddin¹, Sajjad Shafei¹,

Dinidu Perera², Rechana C. N. Remadevi¹, Sharon L. Redmond³, Warren Batchelor⁴, Colin J.

Barrow⁵, Rodney J. Dilley³, Hannes C. Schniepp², Xungai Wang¹ and Rangam Rajkhowa¹*

¹ Deakin University, Institute for Frontier Materials, Geelong, Australia

² Department of Applied Science, William & Mary, Williamsburg, VA, USA

³ Ear Science Institute Australia and Ear Sciences Centre, School of Medicine, University of Western

Australia, Australia

⁴ Bioresource Processing Institute of Australia, Department of Chemical Engineering, Monash

University, Melbourne, Australia

⁵ Life and Environmental Sciences, Deakin University, Waurn Ponds, VIC 3217, Australia

These authors made an equal contribution to this work

* Corresponding author:

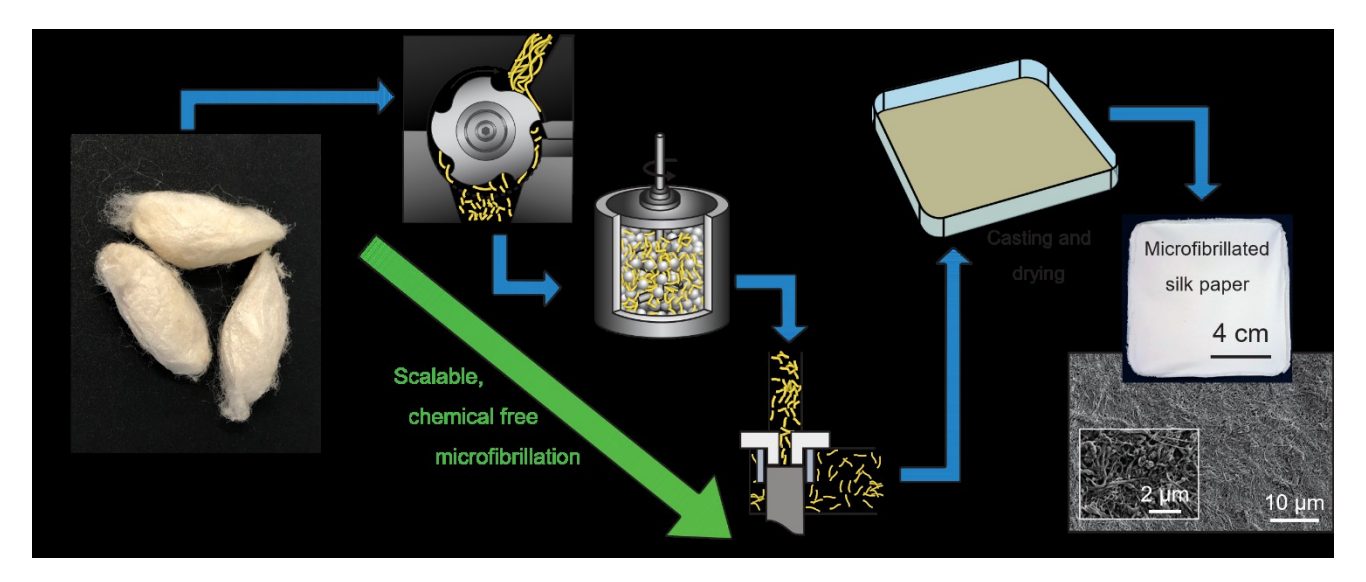
Tel.: +61 3 5227 3427

Email address: rangam.rajkhowa@deakin.edu.au

Abstract

The exfoliation of silk fiber is an attractive method to produce silk micro and nano fibers that retain the secondary structure of native silk. However, most fibrillation methods used to date require the use of toxic and/or expensive solvents and the use of high energy. This study describes a low cost, scalable method to produce microfibrillated silk nanofibers without the use of toxic chemicals by controlling the application of shear using commercially scalable milling and homogenization equipment. Manipulation of the degumming conditions (alkaline concentration and degumming temperature) and the shear in milling and/or homogenization enabled control over the degree of fibrillation. The microfibrillated silk was then characterized to determine structural change during processing and the stability of the resulting suspensions at different pH. Silk nanofibers obtained from milling degummed silk were characterized using atomic force microscopy. Nanofibers obtained both with and without high pressure homogenization were then used to produce silk "protein paper" through casting. Silk degumming conditions played a critical role in determining the degree of microfibrillation and the properties of the cast silk papers. The silk papers produced from homogenized nanofibers showed excellent mechanical properties, high water absorption and wicking properties. The silk papers were excellent for supporting the attachment and growth of human skin keratinocytes, demonstrating application possibilities in healthcare such as wound healing.

Graphical abstract



Introduction

Silk, like some other strong natural fibers, derives its remarkable mechanical properties from its highly ordered hierarchical assembly of nanofibers. The basic sub-structure of silk fiber consists of anti-parallel β -sheet nanocrystals embedded in a less ordered, semi-amorphous phase. These domains arrange into the form of nanofibrils and are aligned as a result of shear forces applied during spinning from the silk gland. Silk nanofibrils are, in turn, packed together in hierarchal bundles with strong cohesive forces to form the silk fibroin fiber. The unique mixture of toughness and extensibility of silk is derived from this highly ordered structure; when stress is applied to the fiber, the β -sheet nanocrystals embedded within the nanofibrils interlock to resist extension, inducing strain hardening, distributing load evenly between nanofibrils across the entire fiber. $^{2, 6-8}$

The availability of nano dimensioned sub-units within a silk fiber provides the opportunity to obtain novel nano featured materials for applications, from nonwoven cell scaffolds, to electronic and environmental applications. Approaches to date have used either bottom up 11, 12 or top down processing. Bottom up processes involve the production of nano fibers from dissolved silk using forced assembly methods such as electrospinning (reviewed in 10), or through the self-assembly of nano fibers from solution. However, dissolving silk and then reassembling it destroys silk's hierarchical structure, resulting in materials that tend to be weak and brittle. In addition, the need to use toxic chemicals to dissolve silk and their separation by slow dialysis process makes the process challenging for industrial production. There are therefore considerable advantages to producing nano fibers directly from native silk fibers (top down processing).

One area of top-down processing that is receiving some attention is the exfoliation of silk fibers to release mesoscale structures; i.e. submicron nanofiber bundles, ^{9, 14-16, 20-22} effectively moving back one step in silks structural hierarchy. Such methods are appealing since nanofibers retain the native structure (and mechanical properties). ²⁰ There is therefore great potential to produce strong, robust materials from exfoliated or as we refer to as microfibrillated silk. However, the production of silk

nano fibers using the exfoliation route is in its infancy compared with other biopolymers such as cellulose or chitin.²⁰

Several approaches to silk microfibrillation have been demonstrated, ranging from high energy ultrasonication to partial dissolution and liquid exfoliation, to mechanical grinding (Table 1).

Many methods had to rely on chemicals which are either toxic and/or require additional steps to separate from the manufacturing system (Table 1, references 13, 16, 25, 26). Other methods achieve fibrillation mostly from surface still having a large amount of large fibers that require separation using centrifugation with inherent drawback of poor yield, lengthy process and difficulty to control and implement in industrial scale. It is also encouraging to note that water-only based milling methods have been used, but with limited control on nano fiber size (Table 1, references 17, 23, 24, 28). The current state of research on nano silk fiber fabrication and application is far behind compared to production of cellulose nano fiber and their application, which has reached to the level of commercial production. This gap has motivated us to investigate this work. Moreover silk being a protein has many functional amino acids for chemical modification and biding of biomolecules compared to cellulose. Besides, the established advantages of silk for many biomedical, biosensing and other biotechnolotial applications, provides scope to research for silk nano fibers fabrication and applications following the widely used and advanced exfoliation method for cellulosic materials.

Table 1: Summary of the published approaches to silk microfibrillation.

| Year | Ref. | Silk type | Fibrillation technique | Reported nanofibre diameter | Advantages | Disadvantages |
|------|------|---|---------------------------------|-----------------------------------|---------------------------------------|---|
| 1997 | 26 | B. mori | Hand beating of silk in NaOH | Unknown | Simple, no organic solvents required | Labour intensive |
| 2007 | 23 | Spider silk (Ornithoctonus huwena) and B. mori silk | Ultrasonication | 25 – 60 nm | Simple, rapid, requires no chemicals. | Low yield due to large quantity of water required (0.05 g silk in 100 mL water) |

| 2014 | 13, 27 | B. mori | CaCl ₂ – formic acid exfoliation (dissolution to nanofibril scale) HFIP exfoliation followed by | $20 - 170 \text{ nm}$ $20 \pm 5 \text{ nm}$ | Liquid dissolution enables easy reprocessing (eg. Into membranes, electrospinning etc.). Produces very fine nanofibers with tight | Use of corrosive organic solvent (formic acid). Nanofibrils are not stable in CaCl ₂ – formic acid (reported to be less than 6 h). ¹⁶ Use of HFIP limits scaling up |
|------|--------|---|---|---|--|---|
| | | | ultrasonication | | very high concentrations of nanofibrils can be made in HFIP. 15 | due to the prohibitive cost of HFIP. |
| 2018 | 14 | B. mori Tussah silk (species name not provided) | Liquid exfoliation using Urea/GuHCl (deep eutectic solvent) followed by ultrasonication | 20 – 100 nm | Relatively safer chemicals used | Low yield, particularly for fine nanofibres - large quantities of solvent needed (1:100 silk:solvent) |
| 2018 | 9 | Antheraea pernyi | Partial dissolution in NaClO followed by homogenisation then ultrasonication. | 13 ± 4 nm up to 200-300 nm (dependant on energy input) | No organic solvents required. Tight size distribution. | Low yield, particularly for small nanofibers. Use of sodium hypochlorite may damage nanofibers through oxidation. |
| 2018 | 29 | B. mori | Liquid exfoliation using NaOH/urea | Ribbons of 25 nm × 0.4 nm | Mild conditions (no organic solvents) | Time - requires 3 days at -12 °C. |
| 2019 | 24 | B. mori | Liquid exfoliation in 8.8 M urea | 200 to 400 nm | No organic solvents required. | Requires 30 days to exfoliate nanofibrils. Requires large amounts of urea (8.8 M = 529 g/L) |
| 2019 | 17, 30 | B. mori | Mechanical energy (wet grinding) | 150-200 nm | No organic solvents required. | Limited evidence of isolation of the fibrillated fibres, unclear if the milled fibres form a colloidal suspension (for processing into new materials). |
| 2020 | 25 | B. mori | Swelling in CaCl ₂ / CH ₃ CH ₂ OH/H ₂ | 287.7 ± 75 nm | Rapid, relatively low energy. | Still requires the use of CaCl ₂ and ethanol |

| | O followed by mechanical | | |
|--|--------------------------|--|--|
| | shearing (high | | |
| | speed blender) | | |

A simple and scalable alternative to exfoliate silk is the use of milling or homogenization without needing any harsh chemical agents. We have, in the past, developed a range of physical treatments to produce submicron particles directly from fibers (keeping the crystallinity of silk intact) with little or no chemical treatment. 31-34 Such milling methods were modified for this study to serve as pretreatments for fabrication of exfoliated fibers. An additional benefit of using purely physical processing is that it can be adapted for any silk variety, including semi-domestic species such as the Eri silk (from *Samia cynthia ricini* silkworms) used in this work and other wild varieties that show poor solubility in the solvent systems commonly used with *B. mori* silk. Difficulty in the dissolution of non-mulberry silk often forces researchers to obtain solution from silk gland. However, collection of silk from gland tissue is not feasible for commercial production due to logistical, economical and ethical issues. Besides, a solution-based approach cannot achieve the natural self assembled structure present in a native silk fiber that provides silk's outstanding mechanical properties in both dry and wet states. Our approach may offer advantages, for example fibroin from some silk varieties contains the RGD peptide for cell attachment, which may be of advantage when producing scaffolds for cell types that respond to this signal. 35-37

In addition to fundamental studies on the exfoliation of submicron or nanofibril scale materials, microfibrillated silk can produce a stable suspension and, when assembled through casting or filtration, can form free-standing materials due to entanglement of fibrillated fibers and strong physical interaction between them after drying. Such material can essentially be considered a silk "paper" since the process is similar to the cellulose paper-making process. These silk papers may be useful not only for biomedical materials, but for other applications such as for filtration devices; the use of silk, which can be easily functionalized due to presence of variety of amino acids, may provide benefits to achieve specific properties based on application needs.

The aim of this study was therefore to demonstrate that Eri silk microfibrillated fibers are suitable to form structurally stable and strong silk "protein papers". All processes were carried out in water and chemical processing was limited to use of very dilute sodium carbonate in the degumming step and during the milling process to encourage fibrillation. Compared with sonication, milling and homogenization are low energy and are highly scalable thanks to the availability of commercial scale equipment already used in various industries. More recently, stone grinding has been used to fibrillate silk fibers and produced films and claimed substantial cost savings compared to bottom up approach to produce silk films. 17, 30 We have adopted a similar approach in this work but use our own milling approach followed by high pressure homogenization to produce much finer nano fibers than reported in the past. The nano fibers were then used to produce papers with much better mechanical properties than those reported by Yamada et al.. We have recently reported fabrication details of our scalable and sustainable approach from *Bombyx mori* silk without using any chemicals and achieving nano fiber of high aspect ratio and suspension stability.³⁸ This study used a systematic approach to investigate changes in degumming conditions on fibrillation by milling with or without the subsequent step of homogenization. The physical and mechanical properties of the paper samples were then characterized. Silk papers were also used as scaffolds to grow cells to establish the cytocompatibility of the material and to determine its suitability for potential biomedical applications.

Materials and Methods

Degumming and fibrillation of silk fibers

Raw cocoons without pupae from the multivoltine domesticated *S. cynthia ricini* silkworm (Eri silk) were purchased from Rudrasagar Silk Ltd, India. Cocoons were degummed in an Ahiba IR Pro rotary dying machine (Datacolor, Lawrenceville, USA). All degumming was conducted using sodium carbonate (Na₂CO₃) and unscented olive oil soap (Vasse Virgin, Wilyabrup, Western Australia, Australia) as a wetting agent. A range of sodium carbonate concentrations in degumming were tested in order to determine their effect on silk fibrillation. Degummed fibers were chopped with a rotary

Pulverisette 19 cutter mill (Fritsch Gmbh, Germany) fitted with a 0.2 mm grid. An HSA attritor (Union Process, USA) containing Yttrium treated zirconium oxide grinding media was used for wet grinding chopped silk (3% silk in 0.5% sodium carbonate solution) with a stirrer speed of 200 rpm. Water was circulated to prevent over heating during milling. A heating step was carried out at 70 °C for 1 h after milling and the milled short silk fibers were washed with dH₂O until neutral pH was obtained. Finally, a PandaPLUS 2000 laboratory high-pressure homogenizer (GEA, Düsseldorf, Germany) was used as the final stage of microfibrillated silk at 700 bar for 3 passes. The nano fiber fabrication process is summarized in Figure 1.

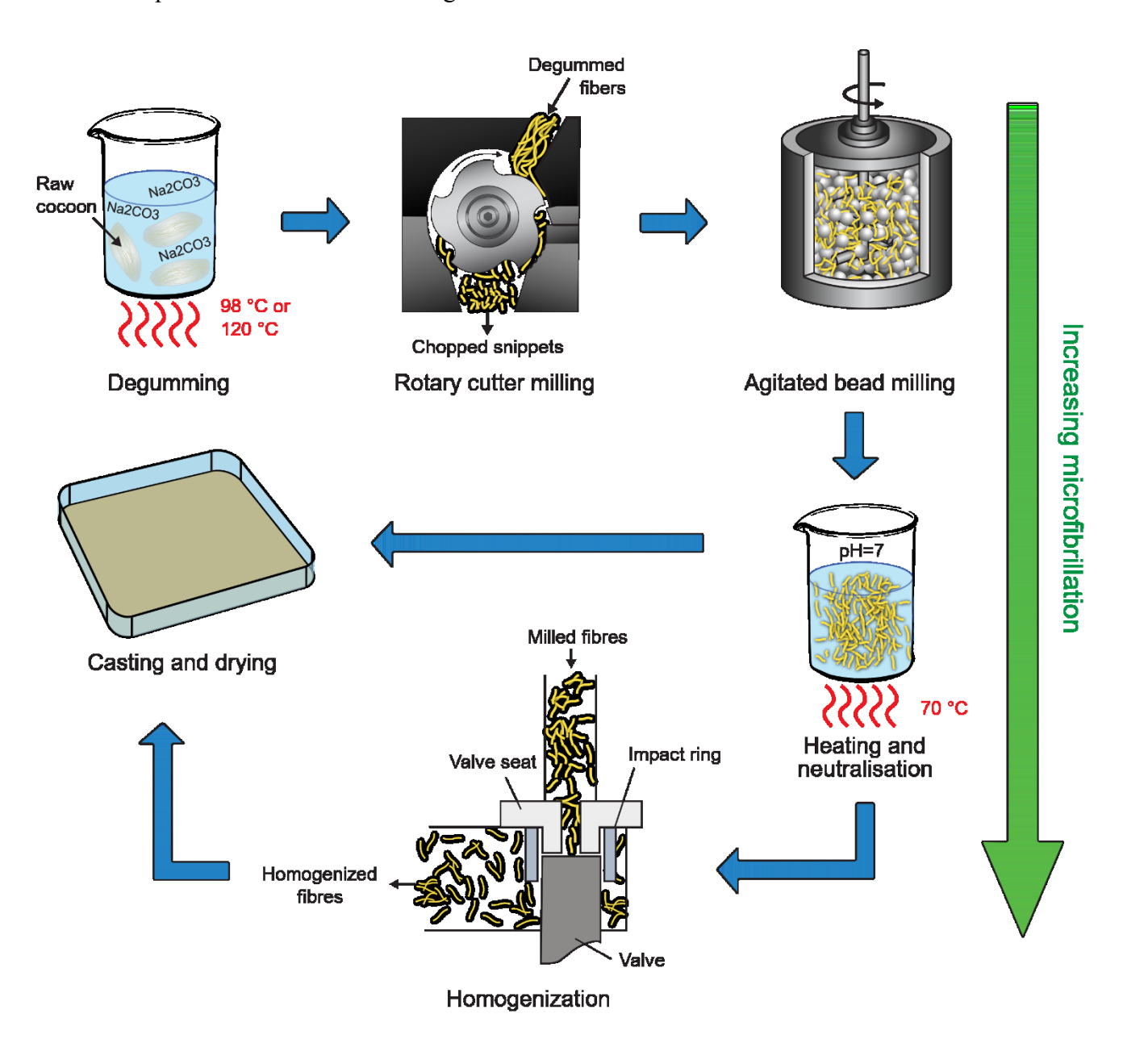


Figure 1: Schematic diagram of silk nanofiber preparation process.

Preparation of silk nano fiber papers

Fibrillated silk from different stages of processing was used for paper making. The fibers were concentrated and washed by centrifuge and then re-suspended to a concentration of 2% w/v in 50 mL of dH₂O. The dispersions were cast into 12 cm² Petri dishes and allowed to dry overnight at room temperature. The final weight of the dried paper samples was approximately 1 g.

Characterization of nano fibre suspension and cast papers

Scanning Electron Microscopy (SEM)

The morphology of the scaffolds made under different conditions was visualized using a Supra 55VP field emission scanning electron microscope (Zeiss, Oberkochen, Germany) after coating with a 5 nm layer of gold using an EM ACE600 High Vacuum Sputter Coater (Leica Microsystems, Wetzlar, Germany). Images were acquired using the secondary electron detector at an accelerating voltage of 5 kV and a working distance of 5-7 mm.

Atomic Force Microscopy (AFM)

Dynamic-mode atomic force microscopy (AFM) images were obtained by an NTEGRA Prima Scanning Probe Laboratory (NT-MDT, Zelenograd, Russia) microscope at ambient conditions using the Universal Head (SF005NTF, NT-MDT) and a 100 μ m × 100 μ m × 100 μ m closed-loop piezo scanner (SC100NTF, NT-MDT). The probes used for imaging were HQ:NSC15/Al BS silicon AFM probes (μ masch, Sofia, Bulgaria) with a typical tip radius of 8 nm, a force constant of \approx 40 Nm⁻¹ and a typical resonant frequency of 325 kHz. Three-dimensionally rendered AFM height images were obtained by Blender 3D creation suite,* version 2.8 (Blender Foundation, Amsterdam, The Netherlands).

Nano fiber suspension stability and surface charge

The stability of the nanofibers suspensions was tested by observing settling of fibers over time. Briefly, 10 mL of each fiber suspension (at a concentration of 1% w/v) were stirred well and placed in 20 mL glass vials. Digital photos were taken at 0 hr, 6 h, 24 h, 3 days, 7 days, and 1 month.

To further investigate the stability and surface charge of homogenized SNF suspensions, 15 mL of three diluted suspensions (concentrations of 0.3% w/v) were prepared, centrifuged and resuspended in the prepared buffer at different pH (Table 2). The surface charges of the suspensions at different pH values were measured using a Malvern Zetasizer (Malvern Panalytical, United Kingdom) in disposable folded capillary cells (DTS 1070) under zeta mode. The stability of these nanofiber suspensions was then measured after 48 h of sedimentation in these buffers (Table 2).

Table 2: pH values used for zeta potential experiments, and the buffer used to achieve this pH.

| pН | Buffer details |
|----|---|
| 3 | Citric acid: 0.0805 M; Na ₂ HPO ₄ : 0.0195 M |
| 5 | Citric acid: 0.0489 M; Na ₂ HPO ₄ : 0.0511 M |
| 7 | Citric acid: 0.0174 M; Na ₂ HPO ₄ : 0.0826 M |
| 9 | Na ₂ CO ₃ : 0.0105 M; NaHCO ₃ : 0.0895 M |
| 11 | Na ₂ CO ₃ : 0.087 M; NaHCO ₃ : 0.013 M |

Measurement of surface roughness

The top and bottom surfaces of dried nano fiber papers were imaged using an OLS 4100 Laser Confocal Microscope (Olympus, Tokyo, Japan). Scans were taken at a magnification of 50 × and used to calculate the mean area roughness parameter (Sa). The roughness was determined for at least 3 fields of view for each sample and expressed as the mean ± standard deviation of these measurements. Differences in roughness between the top and bottom surface of each sample were compared statistically using a paired sample t-test using Origin version 2019b (Originlab, Northampton, MA, USA) at the 0.05 significance level.

Aspect ratio measurement

May add from the previous paper

Mechanical properties

Nanofiber paper samples were cut into 10×55 mm strips and tested according to Australian/New Zealand Standard Methods 448 s and 437 s with slight modification. Briefly, the samples were conditioned to $20 \, ^{\circ}\text{C} \pm 2 \, ^{\circ}\text{C}$ and $65\% \pm 2\%$ relative humidity for at least 24 h prior to testing. Conditioning was carried out to avoid influence of moisture on tensile properties. Samples were tested to break on an Instron 5967 tester with 50 N load cell (Instron, Norwood, MA, USA). Samples were tested with a gauge length of 20 mm and a crosshead speed of 2 mm/min. The weight of each sample was measured on a 4 decimal place balance and the tensile index was calculated from tensile strength per unit width (N/m) divided by GSM (g/m²) and express as N·m/g.

Contact angle

Water contact angle of the samples was measured according to ASTM D5946-09 using KSV CAM200 goniometer. A 5 μ L droplet of water was placed on each specimen and images were taken of the droplet on surface at intervals of 0.33 s. Using Young/Laplace method (Attension-theta software version 4.1.9.8), the water contact angle was calculated on each sample \sim 1 s after the droplet was placed on the surface. The average of left and right contact angles was recorded. Images of the droplet on each sample were captured until it was all absorbed and the absorption time was recorded. Average and standard deviation for both contact angles and absorption times were calculated.

Wicking test

Paper samples were cut into 60×10 mm strip and fixed on a steel ruler at 65 mm high and a Petri dish filled with colored dye solution was put underneath the strips. The dye pick-up was measured using another ruler at 15, 30, and 60 min (Figure S2).

Water-vapor transmission rate test

Water-vapor transmission rate was measured using a W3-031 water vapor transmission rate tester (Labthink Instruments Co., Ltd., China). Each paper sample was cut into three discs of 11.04 cm² by a sample cutter and mounted into the test dish (with 2 mL of distilled water). A water vapor permeability method was used with 6 cycles per specimen. Each side of the disc was tested while putting it facing down allowing the moisture to penetrate through. The test temperature was 38 °C, the humidity was 90% RH, and time interval was 5 min.

Silk secondary structure

The secondary structure change in silk during processing was measured using the ATR mode on a LUMOS FTIR microscope (Bruker Biosciences Pty, Australia). For each sample, 128 scans were taken at a resolution of 2 cm⁻¹. The spectra were obtained from 4000 to 600 cm⁻¹, then the secondary structure of the fibroin was quantified following published methods.^{39, 40} The scanned spectra were subjected to a Fourier self-deconvolution and curve fitting process using OPUS 7.2 software (Bruker, Billerica, MA, USA). The deconvolution was performed for the amide I region (1705 - 1595 cm⁻¹) using a Lorentzian model with bandwidth of 25 cm⁻¹ and a noise reduction factor of 0.3. A baseline correction was then carried out, followed by curve fitting using a Gaussian model. The percentage area under each peak was calculated and assigned to side chain, β -sheet, random coil, α -helix, and β -turn for specific regions within 1705 - 1595 cm⁻¹.^{39, 40}

Cytocompatibility

Cell adhesion to silk paper scaffolds was evaluated with immortalized human keratinocyte (HaCaT) cultures. Cells were routinely cultured in Dulbecco's Modified Eagle Medium (High glucose 4.5mg/L) (Gibco) with 10% fetal bovine serum and antibiotic/antifungal (penicillin and streptomycin (5000U/mL, Invitrogen). For the assay, stock cultures were resuspended in DMEM and plated onto pre-wetted samples of test material (10K -50,000 cells on material pre-cut to 7mm diameter discs using a biopsy punch to fit 96-well plates). Samples were cultured for 48 hours in a humidified cell culture incubator at 37°C with 5% CO₂ to allow adhesion, fixed in 10% buffered formal saline,

washed in 1x PBS (Gibco) and stained with DAPI (4',6-Diamidino-2-Phenylindole,

Dihydrochloride) (Molecular Probes). Control wells were cultured onto tissue culture plastic and treated exactly as per the test samples. All materials were imaged on a Nikon Eclipse Ti2 inverted fluorescence microscope with attached Ds-Qi2 monochrome camera (Nikon, Japan). A 10x CFI Plan Fluor objective (NA 0.30, WD 16.0 mm (Nikon Japan)) was used to view materials with images saved as ND2 files using Nikon Elements software (v 5.11.01).

Assessment of cell proliferation was performed using the CellTiter 96 Aqueous One Solution Cell Proliferation Assay (Promega Corporation). Briefly, 10, 000 cells in a total of 100 μL of DMEM were cultured on 7 mm scaffold discs (n=3), along with tissue culture plastic control wells, for 48 hours. 20 μL of assay solution was added to all wells and incubated for 4 hours at 37°C with 5% CO₂. A total of 120 μL was removed from each well and added to a fresh plate. Plates were then read at wavelength of 490 nm absorbance using an Epoch colorimetric plate reader (BioTek). Absorbance is directly proportional to the number of living cells in culture.

Statistics

Data are expressed as mean \pm standard deviation. Where appropriate, results were compared using a one-way ANOVA with Tukey post-hoc analysis using Origin 2019b. Results were considered statistically significant at p \leq 0.05. For simple comparisons between 2 means (for the surface roughness measurements), t-tests were conducted using the 0.05 significance value.

Results and Discussion

In order to investigate the effect of silk processing on the degree of exfoliation and ability to form silk papers, four silk degumming conditions were investigated by changing the temperature and sodium carbonate concentration (2g/L and 5g/L Na₂CO₃ at temperatures of 98 °C and 120 °C) as shown in Figure 2. Silk papers were prepared from pulp after milling with or without subsequent

homogenization from fibers processed using each of these degumming conditions. Degumming conditions were selected based on preliminary experiments. Of the four degumming conditions tested, silk degummed using the mildest degumming conditions (2g/L, 98 °C) did not produce paper after milling without subsequent homogenization (group 1M); fibrillation was evident in this group (see supplementary information, Figure S1a), but the degree of fibrillation caused by milling was insufficient to allow the enough fiber entanglement to form a free-standing paper. Formation of a free-standing paper requires sufficient interaction between fibers. Nano fiber network density and and thus the contact points increase with higher surface area of finer fibers and higher aspect ratio resulted from microfibrillation. Poor fibrillation of group 1M therefore did not result in formation of a free-standing paper. Subsequent homogenization of fibers degummed using these conditions did provide enough fibrillation (Figure S1b) to produce a paper (Figure 2a, sample 1M+H). The extent of fibrillation and the morphology of microfibrils are shown in the AFM images in Fig. 3. Splitting and branching out and formation of network is clearly evident in the image. The magnified AFM image of a sub-micron strand featured in the inset of Fig. 3 also shows that it contains much finer (<50nm) nanofibers and thus represents a nanofiber bundle. Such bundles are fine enough to have a good network and form a strong free standing paper. Similarly, under the most intensive conditions (group 4: 5g/L sodium carbonate and 120 °C degumming temperature) could not form paper (Figure S1g and h). The most likely reason for this is excessive alkaline hydrolysis of fibroin caused by the high sodium carbonate concentration, further mediated by the high temperature. Such aggressive conditions are known to reduce fibroin molecular weight^{41, 42} and produced very weak fibers. ^{41, 43} Milling and homogenization of this highly damaged fibroin resulted in the production of brittle and very short nanofibers (Figure S1g and h), with a lower aspect ratio and hence less number of contact points. These factors led to a brittle paper that collapsed during drying (Figure 2b, samples 4M and 4M+H). Li et al. also reported formation of brittle paper with poor mechanical properties if silk fibers were intensively processed prior to fibrillation.²⁴

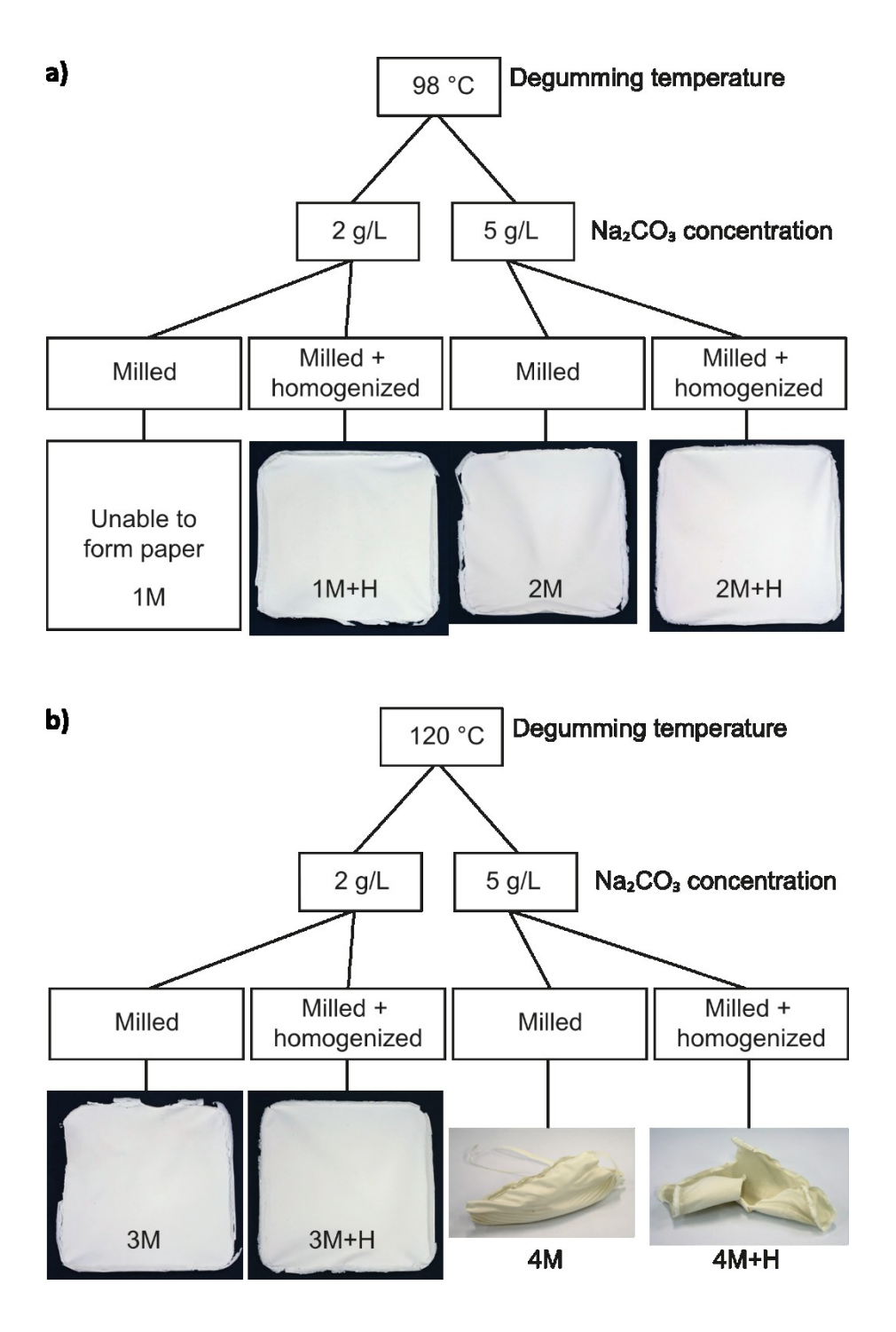


Figure 2: Formation of paper from *P. ricini* silk degummed at 98 °C (a) and 120 °C (b). Treatment conditions are given a code which is used throughout the manuscript. E.g. 1M = Silk nano fiber group 1, milled, 1M+H = group 1, milled and homogenized.

Silk nanofiber (SNF) Paper surface morphology and roughness

SEM images of the top and bottom surfaces of the silk nano fiber papers are presented in Figure 3. Increasing the Na₂CO₃ concentration or degumming produced a higher degree of fibrillation. However, when concentration was increased to 5 g/L together with a degumming temperature of 120 °C, the fibers were severely ruptured along the length during milling, resulting in short fibers as

reflected in the SEM images (see supplementary Figure S1g and h). Such degraded silk could not form good papers as shown in Figure 2 (4M and 4M+H). In all images (Figure 3) top surfaces present the long and entangled nano fibers across the surface of the paper (Figure 3a, d, g, j and m). In contrast, the fibers at the bottom surface of the paper (Figure 3b, e. h, k and n) are shorter and more compact. This difference corresponded with the mean roughness of the paper samples, measured by Laser Confocal Microscope, with the exception of sample 3M+H, the top surface for each paper type (Figure 3c, f, I, 1 and o, black bars) was significantly rougher than the bottom surface (Figure 3c, f, I, 1 and o, grey bars). These differences are most likely due to fiber settling during drying, where fibers that are larger (in diameter) or shorter presumably settle faster rather than becoming entangled within the paper. The bottom surface was also significantly smoother as a result of drying in contact with the smooth Petri dish surface.

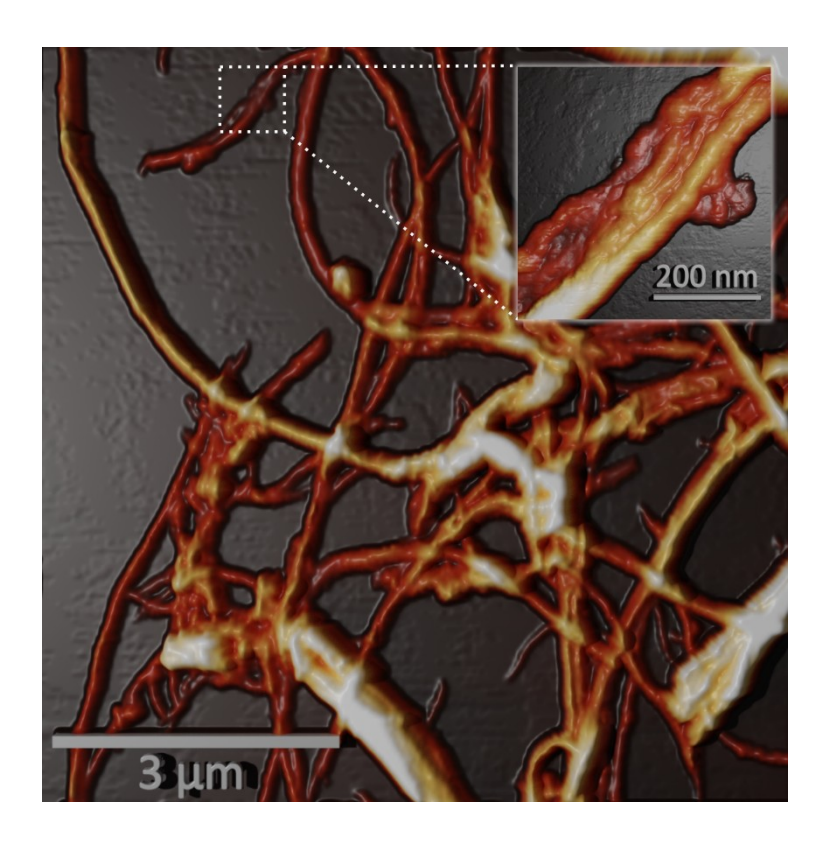


Figure 3: Three-dimensional rendering of an AFM image featuring the fiber network and branching. Inset: AFM scan featuring higher magnification to reveal the thinner nanofibers.

SEM images support that microfibrillation occurred even due to milling alone; however, it was not sufficient for 1M sample to form paper. In the case of 3M, nano fibers were still not separated and remained as a bundle and an example with a width = $8.17 \mu m$ is presented in Figure 3j with a double

headed white arrow; however, their fibrillation was sufficient to form a free standing paper (Figure 2). Significant exfoliation by milling only process was particularly evident in 2M sample; thus milling plays a significant role in the process and can generate nano fibers. Further processing in the homogenization step increased the degree of exfoliation and fibers mostly with sub-micron scale width are evident in 2M+H and 3M+H samples.

Homogenization had the most noticeable impact on reducing roughness of the top surface of the paper, bringing it closer to the roughness of the bottom surface (Figure 3 f vs i and l vs o). Group 3M+H, produced the finest fibers on the top surface (Figure 3m), with widths ranging from under 50 nm to approximately 1 µm. The impact of homogenization is consistent with similar studies on nanocellulose where homogenization was found to be highly effective in reducing fiber diameter and increasing aspect ratio.⁴⁴

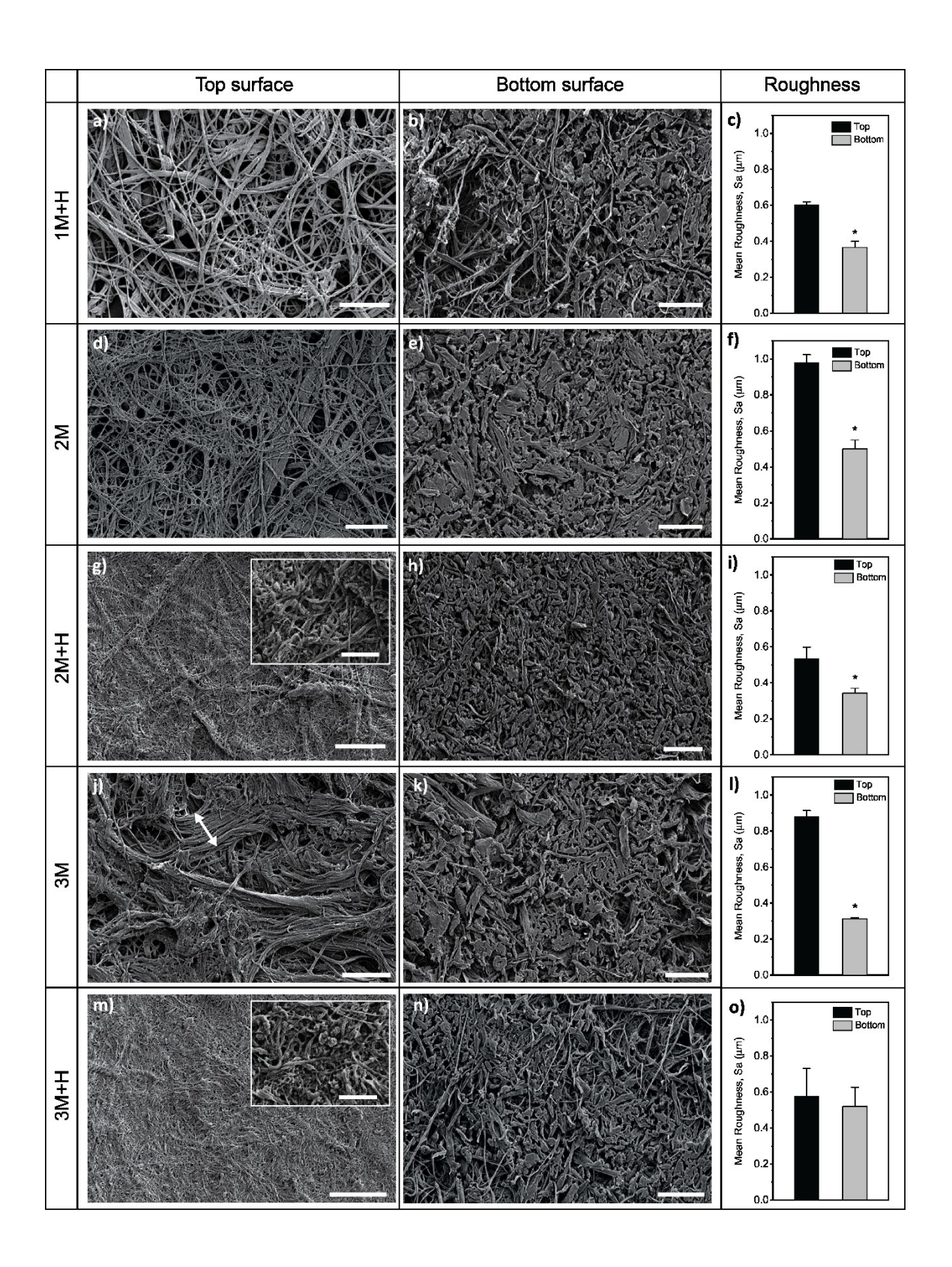


Figure 3: SEM images of the SNF paper on both sides. a) and b) 1M+H top and bottom; c) 1M+H roughness d) and e) 2M top and bottom; f) 2M roughness; g) and h) 2M+H top and bottom; i) 2M+H roughness; j) and k) 3M top and bottom; l) 3M roughness; m) and n) 3M+H top and bottom; o) 3M+H roughness (Scale bars: main images = 10 μ m, inset images = 2 μ m). Double headed white arrow in g) indicates an example of a poorly fibrillated fiber bundle, width = 8.17 μ m. Inset images show a higher magnification view of the larger image. Roughness graphs show mean \pm standard deviation, star symbols on graphs (*) indicates statistically significant difference between the roughness of the top and bottom surface (t-test statistic: P<0.05).

Stability of SNF suspension.

Stability studies of the suspensions were performed to understand the aspect ratios of the SNFs (Figure 4). All fiber suspensions were stable at room temperature for 6 h, and then the sedimentation started, as indicated by the presence of clear water on top of the suspended fibers (Figure 4, red arrows). All homogenized samples remained stable and there was no sign of sedimentation even after one month. The high stability of all of the suspensions in water suggests that the fibers have a high aspect ratio, since sedimentation is prevented by network of fibers and higher aspect ratio improves network formation for a given concentration of fibers in the suspension. 45, 46



Figure 4: Stability of 1% w/v SNF before and after homogenizing. Red arrows indicate the formation of clear zone in the water as the unhomogenized samples settle.

To understand the effects of surface charge of silk nano fibers on the stability of fiber suspensions, we measured zeta potential across the pH range of 3 to 11 (Figure 5a). The isoelectric point of the samples ranged from just under 4 for the 1M+H and 3M+H samples to close to 5 for 2M+H. This is similar to the reported isoelectric point of *B. mori* silk, which is found at pH 3.9 ⁴⁷. The zeta potential is likely to be influenced by the size and morphology of the material since chemistry at material surface can be different compared to the bulk material. The results from this study show that the zeta potential of the nano fibers at pH 7 was between -27 and -29 mV for the three samples (Figure 5); this also falls in line with the reported values for silk, which ranged from -16.5 to -43 mV. ^{11, 48}
Interestingly, the isoelectric point of the nano fiber suspensions changed slightly for fibers prepared with a higher concentration of sodium carbonate during degumming. Perhaps the higher alkali during degumming corresponded with greater fibroin hydrolysis, resulting in an increase in the proportion of amino acids with negative charges on the fiber surface.

The zeta potential data correlated with the sedimentation results. Sedimentation of nanofibers was encouraged by higher zeta potential (Figure 5b). The fibers close to isoelectric points did not settle even after long time whereas sedimentation with clear water above the fibers is visible as the pH shifted away from the isoelectric point. It is likely that the nano fibers formed networks resulting in a higher suspension stability when surface charge was small. As the surface charge increased, there was repulsion breaking the network and eventually the fibers settled with time. It is clear from this study that low zeta potential helped to form a stable network of nano fibers which provided a higher suspension stability. All nano fiber suspensions within the pH range 3-7 had zeta potential below 30 (positive or negative) as shown in Figure 5a. Higher degree of sedimentation at higher alkaline pH could be also from change in density due to water absorption but further studies are warranted to confirm this hypothesis.

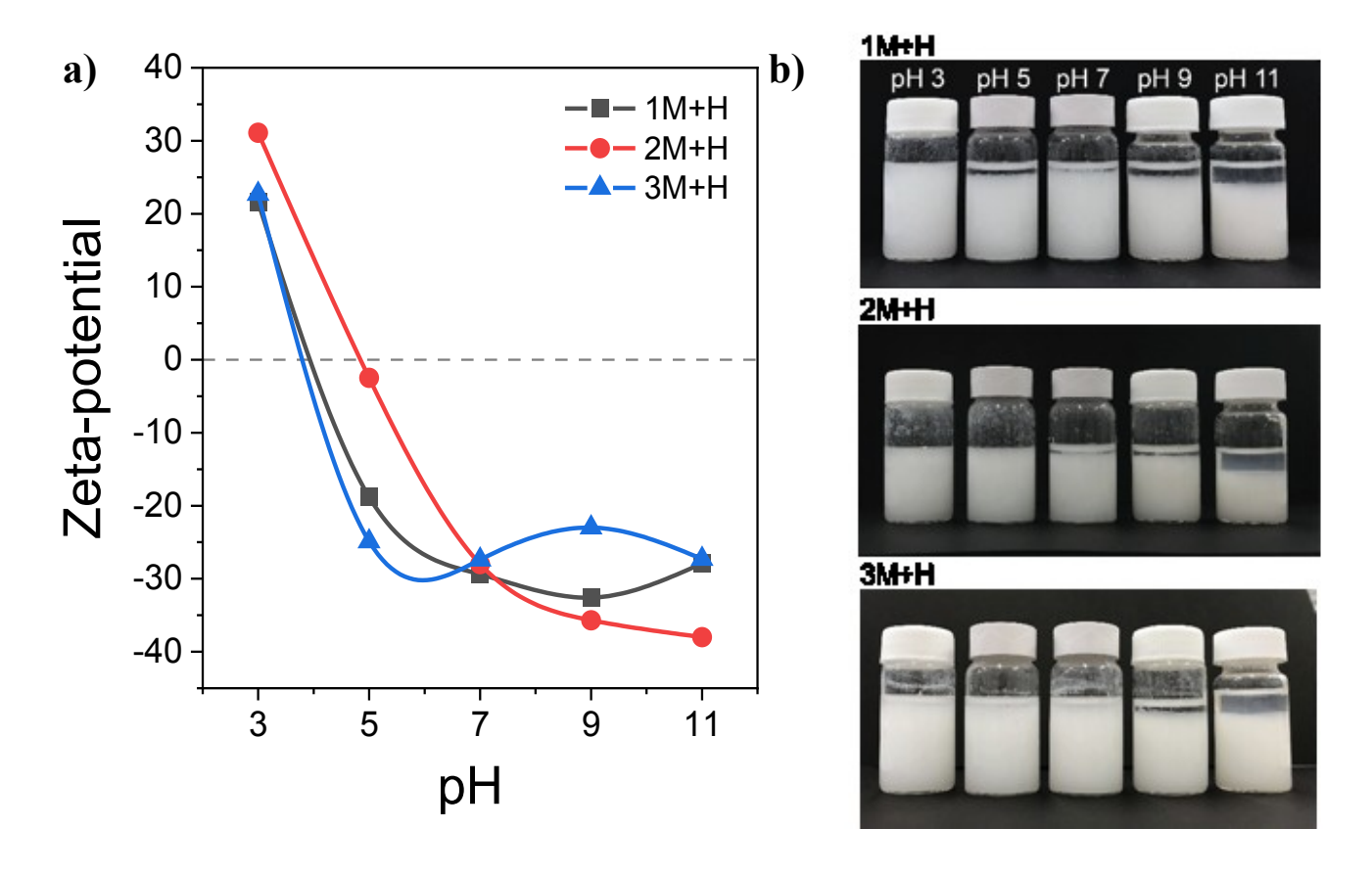


Figure 5: Zeta-potential (a) and pH stability after 48 h of sedimentation of the homogenized solutions (0.3% w/v).

FTIR results and proposed fibrillation mechanism

Secondary structure of silk fibroin plays an important role in the mechanical properties, degradation behavior and many other important aspects for silk materials. FTIR was used to understand if there was any change to the secondary structure of silk during process. The results suggest that regardless of treatment severity, the degumming, milling and homogenization steps preserved β-sheet structures within the silk paper samples, as indicated by the presence of strong peaks around 1697 and 1620 to 1630 cm⁻¹ (Figure 6). For all treatment groups, the milling step introduced a shift in the major β-sheet peak, from 1620 cm⁻¹ for degummed fibers to 1629 cm⁻¹ for all milled and homogenized samples (Figure 6). The most likely explanation for this peak shift is the loss of the weak intermolecular β-sheet peak located between 1616 and 1621 cm⁻¹, ^{39, 49, 50} this result matches our previous finding that attritor milling disrupts intermolecular packing without completely destroying β-sheets. ^{34, 35} The FTIR spectra of the milled vs. milled + homogenized samples were

indistinguishable (Figure 6 M vs M+H samples), suggesting that the homogenization step does not change the fibroin secondary structure.

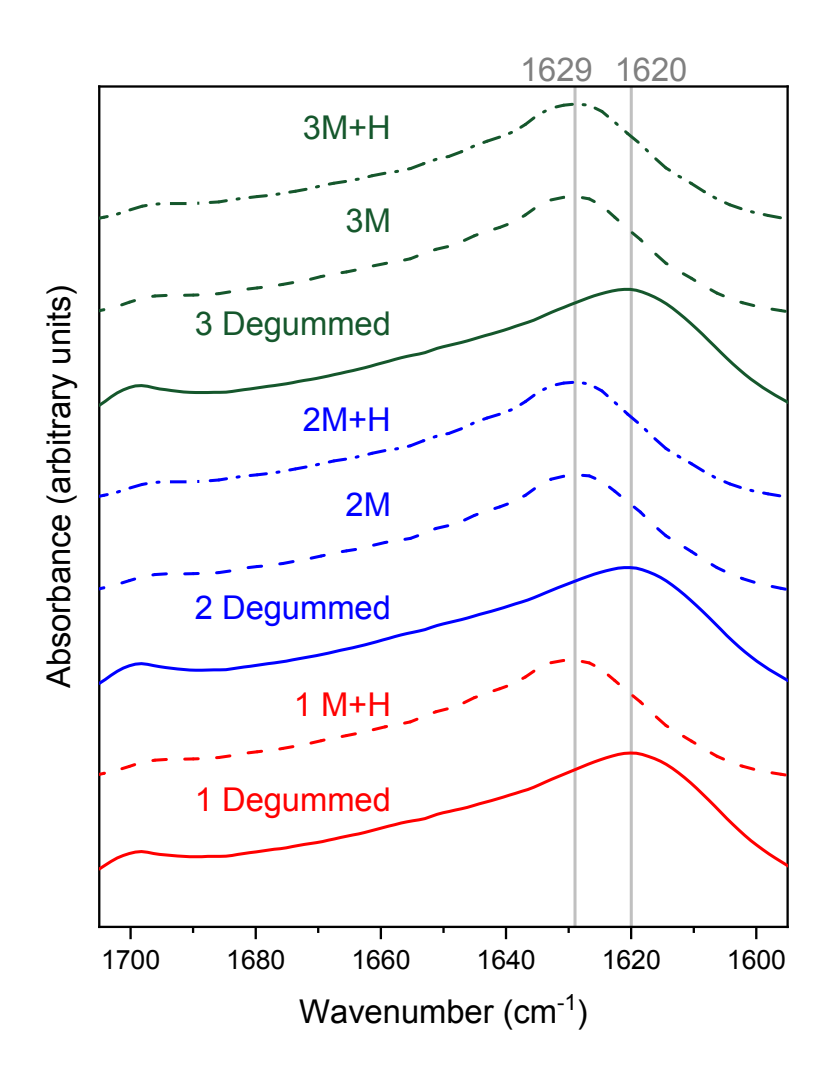


Figure 6: FTIR spectra of the silk paper samples compared with degummed fibers from the same treatment group. Grey vertical lines indicate the position of the β -sheet peak of the samples (1620 cm⁻¹ for all degummed fibers and 1629 cm⁻¹ for all milled and homogenized samples).

In addition to these results, preliminary work established that the cutter mill step and the choice of screen used to filter the cut snippets had a significant impact on fibrillation efficiency and that fibrillation appeared to begin at the cut ends of the snippets. By taking these findings together, a fibrillation mechanism can be proposed. Alkaline degumming is known to cause significant damage to fibroin, ^{42, 43} with the degree of damage relative to the severity of degumming conditions.

Therefore, the more severe the degumming conditions used in this experiment (5 g/L Na₂CO₃ and 120 °C degumming temperature) would result in greater fibroin damage. The defects introduced to

fibroin during degumming presumably create weak points that could form fibrillation sites, explaining the higher degree of fibrillation as degumming severity increased. Following degumming, the production of fiber snippets using the cutter mill increases the proportion of free fiber ends and therefore increases possible fibrillation sites. The media milling step then weakens the intermolecular β-sheet bonding through the application of shear to the fiber snippets. Fibrillation begins at this point but is inefficient, with some fibrillated fibers remaining in clumps (Figure 3i), presumably due to certain degree of cohesion between the bundles and nano fibers (Van der Waal's interactions, non-specific hydrogen bonding etc.). Finally, the application of shear without media through homogenization disrupts this residual intermolecular bonding, producing a much more homogenous dispersion and giving the higher level of microfibillation.

Interaction and transfer of water and water vapor

The water absorption and wettability are important properties to consider if silk papers are to be used for applications where liquid comes in their contact. The silk papers were expected to have different degree of porosity and microchannels based on fiber size and morphology. We looked at the absorption behavior of a water drop as well as water contact angles. The contact angle was recorded immediately after the water drop was placed on the paper surface (~1 s).

The contact angle of the paper samples ranged from 31 ° to 58 ° (Figure 7a). The contact angles of silk papers prepared from homogenized silk nano fibers were higher than the ones prepared from unhomogenized silk (Figure 7a).

All the silk papers absorbed the water drop within 20 sec except group 2M+H (Figure 7b). This sample also had the highest contact angle of all samples tested (58°; Figure 7a), which is approaching the contact angle reported for electrospun *B. mori* silk fiber mats, which is around 75°. The SEM image of the bottom surface (Figure 3b, e, h, k and n) which was used for the water contact angle study also show that fibers presented a compact structure and the surface was less porous. Thus, as expected the porosity of the surface played the key role in water penetration

behavior. Silk papers prepared only by milling without the homogenization step absorbed water immediately due to porous surface with larger fibers. The difference in water penetration properties between the two surfaces, particularly for the paper from sample 2M+H also demonstrates that paper with directional water transmission properties can be produced by adjusting the processing steps to create a more compact surface on one side while leaving the other side porous.

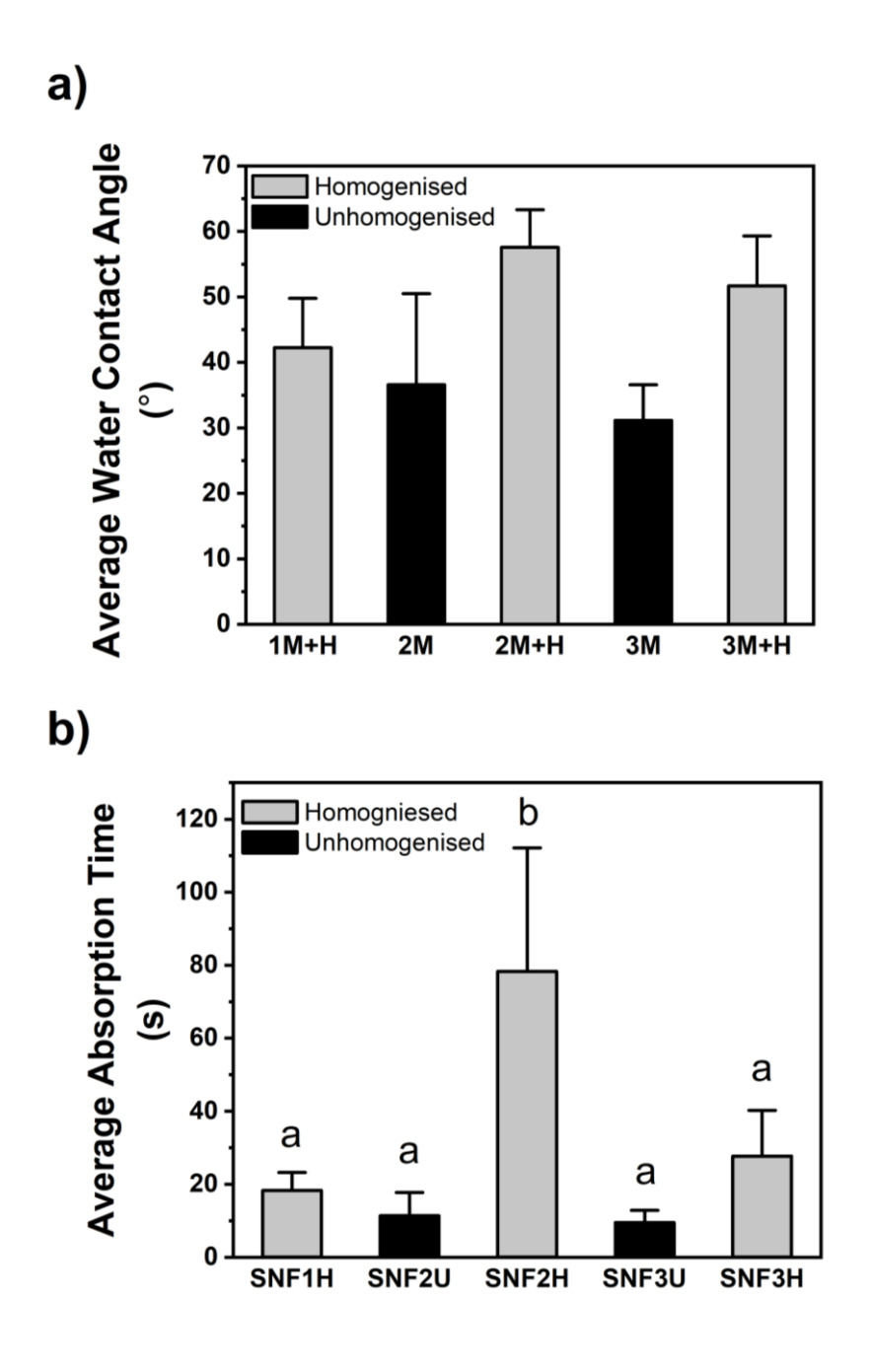


Figure 7: Average water contact angle (a) and average absorption time (b) of the SNF papers. . Letters above the bars (Figure 7b) indicate statistically similar groups

A wicking test was used to further investigate the rise of liquid through the capillary action of the papers (Table 2). Liquid migration was monitored visually by observing the height of color of dye solution at 15 min, 30 min and 60 min; no further movement of the dye front was observed after that. Results presented in Table 3 show that silk paper from homogenized nano fibers provided faster and higher wicking property. The wicking is inversely proportional to the time of absorption. Increasing compactness due to finer nano fibers resulted in a greater number of smaller capillaries and produced superior water transfer properties through the capillaries.

Table 3. Results of wicking testing after certain duration (mm).

| Sample name | Testing duration | | | |
|-------------|------------------|--------|--------|--|
| Sample name | 15 min | 30 min | 60 min | |
| 1M+H | 26 | 26 | 31 | |
| 2M | 18 | 22 | 24 | |
| 2M+H | 26 | 29 | 32 | |
| 3M | 20 | 22 | 24 | |
| 3M+H | 29 | 31 | 32 | |

The water vapor transfer through the paper is useful to understand the barrier properties of the materials. The transfer properties were measured separately for both sides of the paper. The results presented in Table 3 show that the trend is similar to the water absorption tests. Papers prepared from finer homogenized nano fibers allowed less vapor transfer compared to more porous papers prepared from non homogenized silk. Moreover, the bottom side which produced more resistance to water penetration also had slightly more resistance to vapor transfer compared to top side but the difference was not statistically significant. The top side of the 1M+H sample, which was the most porous as reflected in the SEM images, allowed most moisture vapor transfer among the homogenized silk papers. The transmission rate of unhomogenized samples (2M and 3M) was greater than that of the homogenized samples (2M+H and 3M+H) in both sides under same degumming condition. The difference between the transmission rate of top and bottom side in 1M+H was the largest (around 390 g/m²·24 h), while others were all less than 150 g/m²·24 h), reflecting that the structure of 1M+H

was not uniform under this degumming condition. 1M+H also had the largest difference between top and bottom among all homogenized groups. Conversely, the transmission rate of 2M+H was the least among all samples, reflecting that the microfibers prepared by this condition were finer and more even, and produced most compact paper and had the smoothest surface out of all samples (Figure 3).

Table 4. Water-vapor transmission rate of SNF papers.

| Sample name | Top side (g/m ² ·24h) | Bottom side (g/m ² ·24h) |
|-------------|----------------------------------|-------------------------------------|
| 1M+H | 3442.76 ± 326.79 | 3053.28 ± 282.13 |
| 2M | 3279.39 ± 175.14 | 3181.10 ± 210.73 |
| 2M+H | 2838.78 ±149.14 | 2713.43 ± 51.45 |
| 3M | 3673.26 ± 124.69 | 3526.72 ± 122.35 |
| 3M+H | 3266.44 ± 156.74 | 3184.9 ± 125.39 |

Tensile testing

The compactness of the homogenized silk paper samples resulted in significant increase in their tensile stress compared to paper from non-homogenized silk as shown in Figure 8. The tensile stress nearly doubled after homogenizing. The strength of the paper primarily depends on the degree of entanglement, which is enhanced with the degree of micro fibrillation, thereby increasing the number of contact points. It resulted in increase in hydrogen bonding and Van der Waals interaction. The significant increase in strength of group 2 and 3 silk papers compared to group 1 suggests that intensity of degumming played a key role. Although extensive degumming treatment resulted fiber degradation as seen for group 4 samples, some degree of alkali hydrolysis due to higher concentration of alkali (group 2) or increase in temperature (group 3) assisted higher microfibrillation, as reflected in SEM images (Figure 3), and thereby enhanced properties of papers. These mechanical properties exceed those of regenerated nanofiber materials such as electrospun silk mats, which typically have a stiffness of between 1/10th and 1/100th of the highest values reported

here.⁵³ The electrospun silk nanofiber membranes require annealing to render them water stable but he process also make such materials very brittle with elongation at break was in the range 3-7%.⁵¹ Silk papers produced in this work are flexible material and 2M+H had an average elongation at break of 14% (Figure 8).

The tensile index reported here is typically used for measuring tensile properties of papers. It is calculated by normalizing breaking load by weight per square area of paper surface and does not account membrane thickness directly. On the other hand in the case of regenerated silk films tensile stress is normalized by membrane cross sectional area thereby takes thickness into measurement. Increasing compactness in thickness direction would change the cross-sectional area but not weight per square area of a paper surface. Therefore, data presented here cannot be compared directly with tensile stress of regenerated silk materials. However, silk papers prepared in this work are flexible and ductile material, with up to about 15% breaking strain, thereby advantageous for many applications over brittle regenerated silk membranes. Silk films were prepared from micro-fibrillated silk from grinding by Yamada *et al.* but these films appeared very brittle with only about 1% breaking strain.³⁰ This clearly reflects a much higher degree of micro-fibrillation achieved in our work due to specialized milling, addition of high pressure homogenization in the process and control over degumming conditions. There was limited control over density due to casting process used in this work. Other paper making approaches such as vacuum filtration to induce compactness may further enhance density and thereby tensile index and that can be explored in the future.

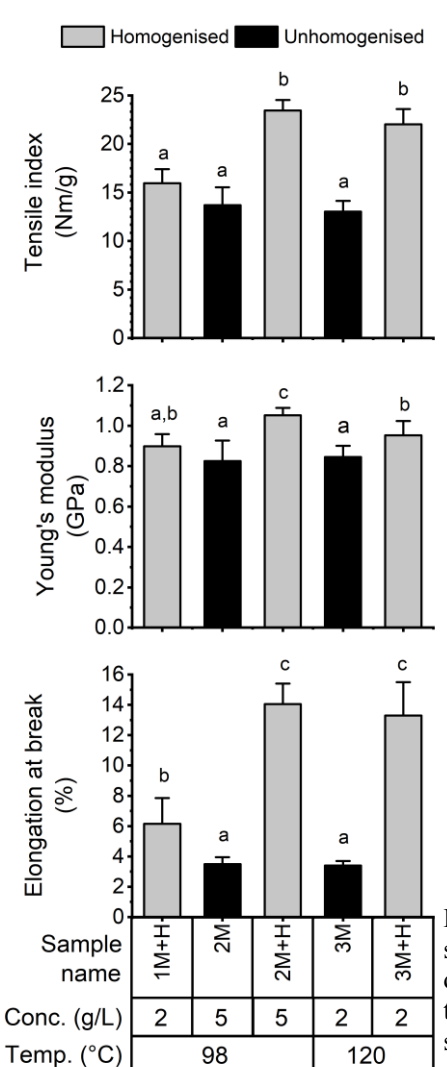


Figure 8: Tensile mechanical properties of the SNF paper samples. NB: Conc. = Na_2CO_3 concentration during degumming, Temp. = Degumming temperature. Letters above the bars indicate statistically similar groups (homogenous subsets) based on a one-way ANOVA with Tukey post-hoc analysis.

Cytocompatibility testing

Human epidermal keratinocytes were found to adhere on all silk paper materials tested. Qualitatively the paper presented a fibrous surface to which the cells adhered closely and spread to form a flattened epithelial monolayer (Figure 9), which at the high density seeding appeared confluent. The presence of mitotic figures (Figure 9b, white arrows) indicated that cells were able to proliferate on

the silk surface.

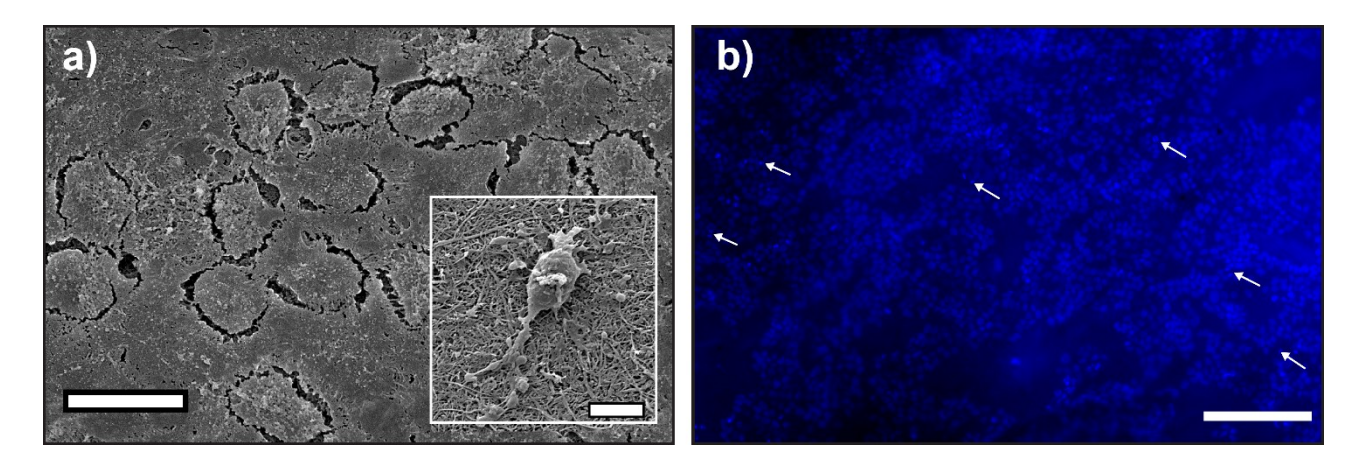


Figure 9 Compatibility with human skin cells. (a) SEM image of human keratinocytes adhering as a confluent monolayer on the ERI silk paper after 48 hours in culture. The islands with dark edges are single cells that have separated during sample processing. The rest of the image consists of continuous cells. (b) Fluorescence micrograph showing high cell density (confluent) is supported and mitotic figures (white arrows, examples shown at higher magnification in inset images) indicating cell proliferation. Scale bars: a) $20~\mu m$; b) = $200~\mu m$, inset images = $20~\mu m$.

An MTT cell proliferation assay was used to compare quantitatively between silk paper samples processed by two of the different degumming methods and with vs. without homogenization (1M+H, 3M and 3M+H; Figure 10). Similar growth outcomes were observed from each degumming method indicating that cell:scaffold interactions were supported under the various degumming conditions.

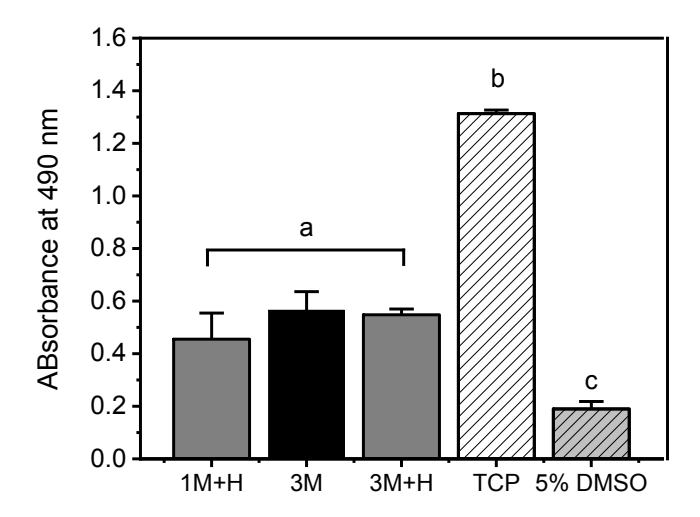


Figure 10 Cell adherence and growth assessed by enzymatic growth assay. TCP = tissue culture plastic (positive control), 5% DMSO, which is cytotoxic, was used as a negative control. Different letters above bars represent differences that are statistically significant (p<0.001) based on a one-way ANOVA with Tukey post-hoc analysis.

Conclusions

Microfibrillation of silk using milling and homogenizing is cost effective, tunable and scalable. By working within the degumming processing window required to fibrillate Eri fibers, this study identified the conditions that produced the best combination of fibrillation without causing excessive damage (or secondary structure changes) to fibroin (98 °C degumming with 2g/L Na₂CO₃, with homogenization: 2M+H). These conditions produced nanofiber papers that had the finest, most consistent fiber diameter that resulted in excellent mechanical properties, high water absorption and biocompatibility. Altering processing conditions enabled tuning of properties such as wicking properties, water vapor transmission rate and contact angle. The flexibility and scalability of this system give it great potential for a range of potential applications including biomaterials and filtration devices.

Acknowledgements

This research was supported by the Australian Research Council (ARC) Research Hub for Future Fibres (IH140100018) and funded by the Australian Government.

References

- 1. Xu, G.; Gong, L.; Yang, Z.; Liu, X. Y., What makes spider silk fibers so strong? From molecular-crystallite network to hierarchical network structures. *Soft Matter* **2014**, *10* (13), 2116-2123.
- 2. Lefevre, T.; Rousseau, M. E.; Pezolet, M., Protein secondary structure and orientation in silk as revealed by Raman spectromicroscopy. *Biophys. J.* **2007,** *92* (8), 2885-95.

- 3. Zhou, C. Z.; Confalonieri, F.; Medina, N.; Zivanovic, Y.; Esnault, C.; Yang, T.; Jacquet, M.; Janin, J.; Duguet, M.; Perasso, R.; Li, Z. G., Fine organization of *Bombyx mori* fibroin heavy chain gene. *Nucleic Acids Res.* **2000**, *28* (12), 2413-9.
- 4. Greving, I.; Cai, M.; Vollrath, F.; Schniepp, H. C., Shear-Induced Self-Assembly of Native Silk Proteins into Fibrils Studied by Atomic Force Microscopy. *Biomacromolecules* **2012**, *13* (3), 676-682.
- 5. Jin, H. J.; Kaplan, D. L., Mechanism of silk processing in insects and spiders. *Nature* **2003**, 424 (6952), 1057-1061.
- 6. Keten, S.; Xu, Z.; Ihle, B.; Buehler, M. J., Nanoconfinement controls stiffness, strength and mechanical toughness of beta-sheet crystals in silk. *Nat. Mater.* **2010**, *9* (4), 359-67.
- 7. Thiel, B. L.; Guess, K. B.; Viney, C., Non-periodic lattice crystals in the hierarchical microstructure of spider (major ampullate) silk. *Biopolymers* **1997**, *41* (7), 703-719.
- 8. Giesa, T.; Arslan, M.; Pugno, N. M.; Buehler, M. J., Nanoconfinement of spider silk fibrils begets superior strength, extensibility, and toughness. *Nano Lett.* **2011,** *11* (11), 5038-46.
- 9. Zheng, K.; Zhong, J. J.; Qi, Z. M.; Ling, S. J.; Kaplan, D. L., Isolation of Silk Mesostructures for Electronic and Environmental Applications. *Adv. Funct. Mater.* **2018**, *28* (51).
- 10. Zhang, X.; Reagan, M. R.; Kaplan, D. L., Electrospun silk biomaterial scaffolds for regenerative medicine. *Adv. Drug Del. Rev.* **2009**, *61* (12), 988-1006.
- 11. Bai, S.; Liu, S.; Zhang, C.; Xu, W.; Lu, Q.; Han, H.; Kaplan, D. L.; Zhu, H., Controllable transition of silk fibroin nanostructures: An insight into in vitro silk self-assembly process. *Acta Biomater.* **2013**, *9* (8), 7806-7813.
- 12. Dong, X.; Zhao, Q.; Xiao, L.; Lu, Q.; Kaplan, D. L., Amorphous Silk Nanofiber Solutions for Fabricating Silk-Based Functional Materials. *Biomacromolecules* **2016**, *17* (9), 3000-3006.
- 13. Zhang, F.; Lu, Q.; Ming, J.; Dou, H.; Liu, Z.; Zuo, B.; Qin, M.; Li, F.; Kaplan, D. L.; Zhang, X., Silk dissolution and regeneration at the nanofibril scale. *J. Mater. Chem. B* **2014**, *2* (24), 3879.

- 14. Tan, X.; Zhao, W.; Mu, T., Controllable exfoliation of natural silk fibers into nanofibrils by protein denaturant deep eutectic solvent: nanofibrous strategy for multifunctional membranes. *Green Chem.* **2018**, *20* (15), 3625-3633.
- 15. Ling, S.; Qin, Z.; Li, C.; Huang, W.; Kaplan, D. L.; Buehler, M. J., Polymorphic regenerated silk fibers assembled through bioinspired spinning. *Nat Commun* **2017**, *8* (1), 1387.
- 16. Ling, S.; Li, C.; Jin, K.; Kaplan, D. L.; Buehler, M. J., Liquid Exfoliated Natural Silk Nanofibrils: Applications in Optical and Electrical Devices. *Adv. Mater.* **2016**, *28* (35), 7783-7790.
- 17. Narita, C.; Okahisa, Y.; Yamada, K., A novel technique in the preparation of environmentally friendly cellulose nanofiber/silk fibroin fiber composite films with improved thermal and mechanical properties. *J Clean. Prod.* **2019**, *234*, 200-207.
- 18. Liu, Y.; Ling, S.; Wang, S.; Chen, X.; Shao, Z., Thixotropic silk nanofibril-based hydrogel with extracellular matrix-like structure. *Biomater. Sci.* **2014**, *2* (10), 1338-1342.
- 19. Ling, S.; Qin, Z.; Huang, W.; Cao, S.; Kaplan, D. L.; Buehler, M. J., Design and function of biomimetic multilayer water purification membranes. *Science Advances* **2017**, *3* (4), e1601939.
- 20. Ling, S.; Chen, W.; Fan, Y.; Zheng, K.; Jin, K.; Yu, H.; Buehler, M. J.; Kaplan, D. L., Biopolymer nanofibrils: Structure, modeling, preparation, and applications. *Prog. Polym. Sci.* **2018**, *85*, 1-56.
- 21. Ling, S.; Kaplan, D. L.; Buehler, M. J., Nanofibrils in nature and materials engineering. *Nat. Rev. Mater.* **2018**, *3* (4), 18016.
- 22. Zhang, W.; Ye, C.; Zheng, K.; Zhong, J.; Tang, Y.; Fan, Y.; Buehler, M. J.; Ling, S.; Kaplan, D. L., Tensan Silk-Inspired Hierarchical Fibers for Smart Textile Applications. *ACS Nano* **2018**, *12* (7), 6968-6977.
- 23. Zhao, H.-P.; Feng, X.-Q.; Gao, H., Ultrasonic technique for extracting nanofibers from natural materials. *Appl. Phys. Lett.* **2007,** *90* (7), 073112.

- 24. Lv, L.; Han, X.; Wu, X.; Li, C., Peeling and Mesoscale Dissociation of Silk Fibers for Hybridization of Electrothermic Fibrous Composites. *ACS Sustainable Chemistry & Engineering* **2019**, *8* (1), 248-255.
- 25. Wang, Q.; Yan, S.; Han, G.; Li, X.; You, R.; Zhang, Q.; Li, M.; Kaplan, D. L., Facile production of natural silk nanofibers for electronic device applications. *Compos. Sci. Technol.* **2020**, *187*, 107950.
- 26. Hata, T.; Kato, H., Fibrillation of silk fibers, its treatment method and producing of silk paper subtitle in Japanese. *The Journal of Sericultural Science of Japan* **1997**, *66* (2), 132-135.
- 27. Zhang, F.; You, X.; Dou, H.; Liu, Z.; Zuo, B.; Zhang, X., Facile Fabrication of Robust Silk Nanofibril Films via Direct Dissolution of Silk in CaCl2–Formic Acid Solution. *ACS Applied Materials & Interfaces* **2015**, *7* (5), 3352-3361.
- 28. Ling, S.; Jin, K.; Kaplan, D. L.; Buehler, M. J., Ultrathin Free-Standing Bombyx mori Silk Nanofibril Membranes. *Nano Lett.* **2016**, *16* (6), 3795-3800.
- 29. Niu, Q.; Peng, Q.; Lu, L.; Fan, S.; Shao, H.; Zhang, H.; Wu, R.; Hsiao, B. S.; Zhang, Y., Single Molecular Layer of Silk Nanoribbon as Potential Basic Building Block of Silk Materials. *ACS Nano* **2018**, *12* (12), 11860-11870.
- 30. Okahisa, Y.; Narita, C.; Yamada, K., Preparation of Silk-Fibroin Nanofiber Film with Native β-Sheet Structure via a Never Dried-Simple Grinding Treatment. *Journal of Fiber Science and Technology* **2019**, *75* (4), 29-34.
- 31. Rajkhowa, R.; Wang, L. J.; Wang, X. G., Ultra-fine silk powder preparation through rotary and ball milling. *Powder Technol.* **2008**, *185* (1), 87-95.
- 32. Rajkhowa, R.; Wang, L.; Kanwar, J.; Wang, X., Fabrication of ultrafine powder from eri silk through attritor and jet milling. *Powder Technol.* **2009**, *191* (1–2), 155-163.
- 33. Rajkhowa, R.; Hu, X.; Tsuzuki, T.; Kaplan, D. L.; Wang, X., Structure and biodegradation mechanism of milled *Bombyx mori* silk particles. *Biomacromolecules* **2012**, *13* (8), 2503-12.

- 34. Rajkhowa, R.; Wang, L.; Kanwar, J. R.; Wang, X., Molecular weight and secondary structure change in eri silk during alkali degumming and powdering. *J. Appl. Polym. Sci.* **2011**, *119* (3), 1339-1347.
- 35. Bhardwaj, N.; Rajkhowa, R.; Wang, X.; Devi, D., Milled non-mulberry silk fibroin microparticles as biomaterial for biomedical applications. *Int. J. Biol. Macromol.* **2015**, *81*, 31-40.
- 36. Bhardwaj, N.; Singh, Y. P.; Devi, D.; Kandimalla, R.; Kotoky, J.; Mandal, B. B., Potential of silk fibroin/chondrocyte constructs of muga silkworm *Antheraea assamensis* for cartilage tissue engineering. *J. Mater. Chem. B* **2016**, *4* (21), 3670-3684.
- 37. Patra, C.; Talukdar, S.; Novoyatleva, T.; Velagala, S. R.; Muhlfeld, C.; Kundu, B.; Kundu, S. C.; Engel, F. B., Silk protein fibroin from *Antheraea mylitta* for cardiac tissue engineering. *Biomaterials* **2012**, *33* (9), 2673-80.
- 38. Uddin, M. G.; Batchelor, W.; Allardyce, B. J.; Byrne, N.; Barrow, C. J.; Wang, X.; Rajkhowa, R., Preparing Bombyx mori Silk Nanofibers Using a Sustainable and Scalable Approach.

 **ACS Sustainable Chemistry & Engineering 2019.
- 39. Hu, X.; Kaplan, D.; Cebe, P., Determining beta-sheet crystallinity in fibrous proteins by thermal analysis and infrared spectroscopy. *Macromolecules* **2006**, *39* (18), 6161-6170.
- 40. Rajkhowa, R.; Levin, B.; Redmond, S. L.; Li, L. H.; Wang, L. J.; Kanwar, J. R.; Atlas, M. D.; Wang, X. G., Structure and properties of biomedical films prepared from aqueous and acidic silk fibroin solutions. *J. Biomed. Mater. Res. A* **2011**, *97A* (1), 37-45.
- 41. Allardyce, B. J.; Rajkhowa, R.; Dilley, R. J.; Atlas, M. D.; Kaur, J.; Wang, X., The impact of degumming conditions on the properties of silk films for biomedical applications. *Text. Res. J.* **2016**, *86* (3), 275-287.
- 42. Wray, L. S.; Hu, X.; Gallego, J.; Georgakoudi, I.; Omenetto, F. G.; Schmidt, D.; Kaplan, D. L., Effect of processing on silk-based biomaterials: Reproducibility and biocompatibility. *J. Biomed. Mater. Res. B* **2011**, *99B* (1), 89-101.

- 43. Gulrajani, M. L., Degumming of silk. *Review of Progress in Coloration and Related Topics* **1992,** *22* (1), 79-89.
- 44. Ang, S.; Haritos, V.; Batchelor, W., Effect of refining and homogenization on nanocellulose fiber development, sheet strength and energy consumption. *Cellulose* **2019**, *26* (8), 4767-4786.
- 45. Varanasi, S.; He, R.; Batchelor, W., Estimation of cellulose nanofibre aspect ratio from measurements of fibre suspension gel point. *Cellulose* **2013**, *20* (4), 1885-1896.
- 46. Zhang, L. Y.; Batchelor, W.; Varanasi, S.; Tsuzuki, T.; Wang, X. G., Effect of cellulose nanofiber dimensions on sheet forming through filtration. *Cellulose* **2012**, *19* (2), 561-574.
- 47. Malay, O.; Bayraktar, O.; Batigun, A., Complex coacervation of silk fibroin and hyaluronic acid. *Int. J. Biol. Macromol.* **2007,** *40* (4), 387-393.
- 48. Lammel, A. S.; Hu, X.; Park, S. H.; Kaplan, D. L.; Scheibel, T. R., Controlling silk fibroin particle features for drug delivery. *Biomaterials* **2010**, *31* (16), 4583-91.
- 49. Taddei, P.; Monti, P., Vibrational infrared conformational studies of model peptides representing the semicrystalline domains of Bombyx mori silk fibroin. *Biopolymers* **2005**, *78* (5), 249-58.
- 50. Tretinnikov, O. N.; Tamada, Y., Influence of Casting Temperature on the Near-Surface Structure and Wettability of Cast Silk Fibroin Films. *Langmuir* **2001**, *17* (23), 7406-7413.
- 51. Zhang, K.-H.; Ye, Q.; Yan, Z.-Y., Influence of Post-Treatment with 75% (v/v) Ethanol Vapor on the Properties of SF/P(LLA-CL) Nanofibrous Scaffolds. *Int. J. Mol. Sci.* **2012**, *13* (2), 2036-2047.
- 52. Yano, H.; Nakahara, S., Bio-composites produced from plant microfiber bundles with a nanometer unit web-like network. *J. Mater. Sci.* **2004**, *39* (5), 1635-1638.
- 53. Min, B. M.; Jeong, L.; Lee, K. Y.; Park, W. H., Regenerated silk fibroin nanofibers: water vapor-induced structural changes and their effects on the behavior of normal human cells. *Macromol. Biosci.* **2006**, *6* (4), 285-92.

Supplementary information

SEM images on silk solution before and after homogenising.

SEM Jeol Neoscope (Jeol, USA) at an accelerating voltage of 5 kV was used to observe the morphology of each SNF in suspension (Figure S1). It is obvious that the degummed silk fibres (groups 1, 2, and 3) tend to aggregate before homogenising (Figure S1a, c, and e), which are greatly improved after 5 times homogenisation (Figure S1b, d, and f). However, sample group 4, which was prepared with the most severe degumming condition (120 °C, 5 g/L) seems degrade the original silk fibre and there is no consecutive fibre left both before and after homogenising (Figure S1g h).

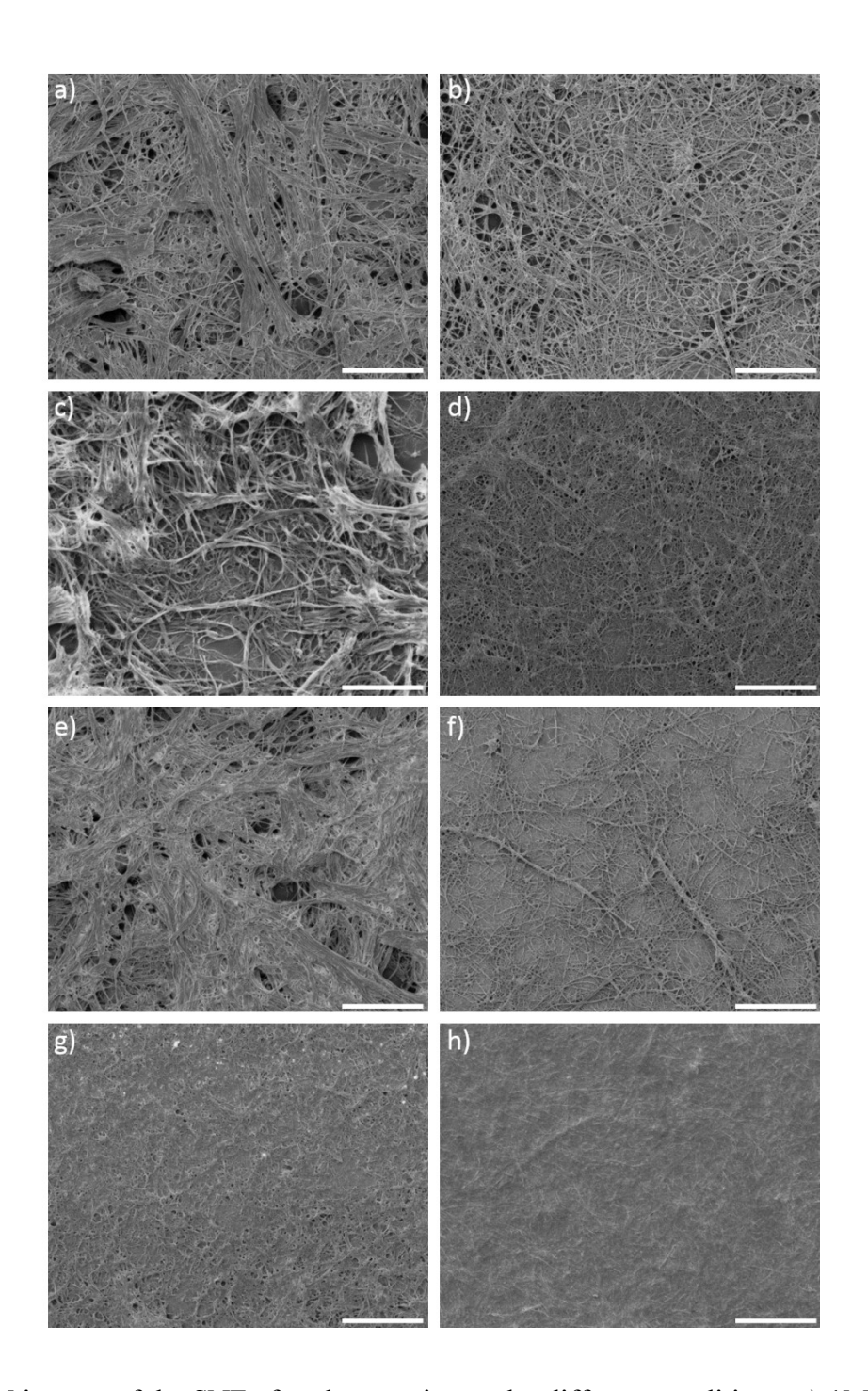


Figure S1: SEM images of the SNF after degumming under different conditions. a) 1M; b) 1M+H; c) 2M; d) 2M+H; e) 3M; f) 3M+H; g) 4M; h) 4M+H (Scale bar: $50 \mu m$).

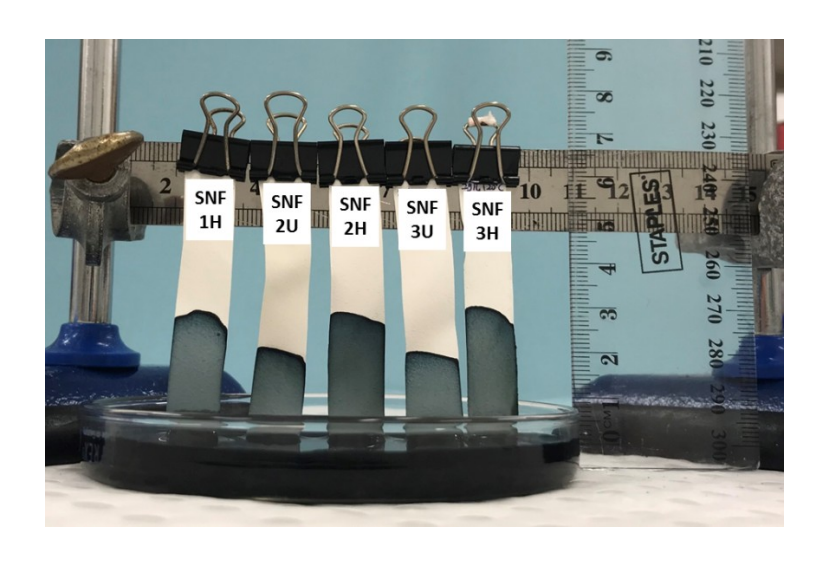


Figure S2. Wick testing on SNF papers